

Magnetic phase diagram of multiferroic and magnetocaloric TmFeO₃

Kirill I. Tkachenko,¹ Piotr Fabrykiewicz,² Aleksandr K. Ovsianikov,^{1,*}

Martin Meven,² Oleg V. Usmanov,¹ Igor A. Zobkalo,¹ Kirill A. Shaykhtudinov,^{3,4}

Konstantin Yu. Terentjev,¹ Sergey V. Semenov,^{3,4} Erik Ressouche,⁵ and Ketty Beauvois⁵

¹*Petersburg Nuclear Physics Institute by B.P. Konstantinov of NRC "Kurchatov Institute", 188300 Gatchina, Russia*

²*Institute of Crystallography, RWTH Aachen University, 52056 Aachen, Germany*

³*Kirensky Institute of Physics, Federal Research Center, Krasnoyarsk 660036, Russia*

⁴*Siberian Federal University, Krasnoyarsk, 660071, Russia*

⁵*Université Grenoble Alpes, CEA, IRIG, MEM, MDN, 38000 Grenoble, France*

(Dated: March 3, 2025)

Neutron diffraction experiments of TmFeO₃ single crystals were performed in the external magnetic fields. The field along *c*-axis increases temperature of spin-reorientation transition T_{SR} from phase $\Gamma 4$ to $\Gamma 2$. Application of the field along *b*-axis led to the decrease of T_{SR} and to the formation of new phases. Based on the temperature and field dependence of the Bragg reflection intensity, the configuration of magnetically induced phases was proposed. The magneto-structural effects were observed.

I. INTRODUCTION

The rare earth orthoferrite family RFeO₃, where R is a rare earth element, has attracted considerable attention for many years. The amazing magnetic properties of these materials are due to two magnetic subsystems – iron and rare earths – and their interactions. In addition to that, these compounds exhibit interesting and intriguing phenomena related to magnetism in them, such as magnetocaloric effects, multiferroicity, optical ultrafast manipulation of magnetic order, etc. The members of the family crystallize in an orthorhombic distorted perovskite structure with the space group *Pnma* (also considered as *Pbnm* in another setting). Orthoferrites RFeO₃ are characterized by a rather high Néel temperatures T_N ranging from 600 K to 740 K [1]. Below T_N , the iron moments become antiferromagnetically ordered, with the sublattices being weakly canted due to the Dzyaloshinskii-Moriya interaction [2, 3], resulting in weak ferromagnetism. In the lower temperature range, the influence of the rare-earth – iron exchange interaction leads to a spin reorientation (SR) transition, the temperature of which varies in a wide range for different R from 3 – 10 K for TbFeO₃ [4] up to 480 K for SmFeO₃ [5].

Until recently, it was believed that ferroelectricity in orthoferrites is not allowed because it is theoretically prohibited by their centrosymmetric *Pnma* structure. However, recent works suggest low-temperature ferroelectricity in DyFeO₃ [6], GdFeO₃ [7], TbFeO₃ [8] and moreover, the observation of the emergence of room-temperature ferroelectricity in SmFeO₃ [9] and YFeO₃ [10]. This multiferroic behavior at higher temperatures opens up the possibility of using of such compounds for switching elements or sensors in the industry applications. Fast manipulation of the spin reorientation in TmFeO₃ has been obtained by laser on ultrafast timescales [11]. This could

be a new direction for spintronics with high speed of magnetic recording.

TmFeO₃ crystallizes in the distorted perovskite structure, described by orthorhombic *Pnma* space group. Below the Néel temperature $T_N = 635$ K [12] Fe³⁺ ions order in $\Gamma 4$ phase with G-type [13] antiferromagnetic order along the *c*-axis. Antisymmetric Dzyaloshinskii-Moriya interaction provides the canting of neighboring antiferromagnetically oriented spins, leading to a net magnetization **m** along the *b*-axis. SR has been observed below $T_{SR} = 93$ K [14, 15], and between 93 and 83 K, the crystal is in the mixed $\Gamma 24$ phase, with **m** laying in the *bc* plane. Below 83 K the magnetic system is in $\Gamma 2$ phase, and G-type antiferromagnetic ordering now directed along axis *b*, while weak ferromagnetic component of type F directed along axis *c*.

One of the most interesting effects associated with orthoferrites is the magnetocaloric effect, which represent itself as the change of temperature of a magnetic substance when subjected to an external magnetic field **B** under adiabatic conditions. For the studied compound, TmFeO₃, the entropy change has a maximum $\Delta S \approx 12$ J/kg·K at 17 K under an applied field of 7 T along the *b* axis [16]. The appearance of ΔS -peaks indirectly demonstrates the possibility of spin reorientation transitions in this field and temperature range in thulium orthoferrite. This requires the study of the phase diagram (*H*, *T*) of TmFeO₃ in external magnetic fields. These types of diagrams help to provide a better understanding of the processes within the Tm subsystem. In addition, the external magnetic field will lead to changes in the energy balance and affect the exchange interaction and anisotropy within the thulium and iron subsystems.

As it is known from a number of previous works on orthoferrites (e.g. [17, 18]), the exchange interaction within the Fe-sublattice plays the main role in the formation of the magnetic structure below T_N . For TmFeO₃ the strongest interaction is the superexchange one through O between the nearest neighbors in the Fe-chains along the *b*-axis and within the *ac*-plane $J_b^{\text{Fe}} = 5.15$ meV and

* ovsianikov_ak@pnpi.nrcki.ru

$J_{ac}^{\text{Fe}} = 4.74$ meV respectively [17]. The exchange field from ordered Fe^{3+} subsystem induces an ordered magnetic moment on Tm^{3+} ions, which is very weak at the temperature above T_{SR} , but becomes more noticeable below spin-reorientation transition [19]. Thus, when the temperature is decreased, the exchange between Fe and Tm sublattices, $J^{\text{Fe-Tm}}$ becomes effective, which leads to spin reorientation transition.

II. EXPERIMENTAL PART

High quality single crystals of TmFeO_3 were grown by the flux method [20] using the optical floating zone technique (FZ-4000, Crystal Systems Corporation) with the natural isotope mixture. X-Ray studies were performed at the Rigaku SmartLab diffractometer at the Petersburg Nuclear Physics Institute (PNPI). These measurements were performed with wavelength 1.54 \AA , 2θ range $20^\circ - 135^\circ$ and the temperature range $T = 50 - 300 \text{ K}$ using powder obtained by grinding of the crystal. Refinement of crystal structure was made using the FullProf Suite software package [21]. Single crystal with cylindrical shape and dimensions of $4 \times 4 \times 8 \text{ mm}^3$ was used for the neutron studies. The neutron diffraction experiments were performed at the Institut Laue-Langevin. The orientation of the crystal was obtained by OrientExpress [22]. This is an automated Laue neutron diffractometer based upon two high-performance image-enhanced CCD cameras coupled to a large-area neutron scintillator and allows fast orientation of the crystal. Magnetic structure studies were performed on diffractometer D23 [23] in external magnetic fields with wavelength 1.28 \AA . Two sets of measurements were made for the direction of magnetic fields along crystal axes b and c with constant field values. For both sample orientations, sets of selected peaks were measured for each combination of temperature 2, 20, 40, 60, 75, 88, 100 K and magnetic field 0, 0.5, 1, 2, 3, 4, 5, 5.8 T. In addition, for both sample orientations, we measured intensities of selected peaks at temperatures 80, 90, 95, 105, and 110 K without magnetic field; this temperature interval includes the temperature range of Fe spin reorientation. Furthermore, two sets of all available reflections (about 500) at temperature $T = 20 \text{ K}$ were collected for two different sample orientations. The program Mag2Pol [24] was used then to calculate and refine the magnetic structure.

III. RESULT AND DISCUSSION

A. Structure study

Our X-ray studies confirmed that the crystal structure of TmFeO_3 is described by the space group $Pnma$ #62 IT [25] at all temperatures of measurement. In this structure Fe-ions occupy position $4b$, Tm – $4c$, O1 and O2 – $4c$ and $8d$ respectively. Obtained parameters of the

TABLE I: Crystal structure of TmFeO_3 at different temperatures, X-ray powder data, $Pnma$ setting.

TmFeO_3		300 K	150 K	85 K	50 K
a [Å]		5.5721(2)	5.5679(2)	5.5655(2)	5.5650(2)
b [Å]		7.5823(2)	7.5761(3)	7.5740(3)	7.5732(3)
c [Å]		5.2468(2)	5.2429(2)	5.2415(2)	5.2407(2)
Fe ($4b$)	x	0.5000	0.5000	0.5000	0.5000
	y	0.0000	0.0000	0.0000	0.0000
	z	0.0000	0.0000	0.0000	0.0000
Tm ($4c$)	x	0.0690(2)	0.0693(2)	0.0693(2)	0.0691(2)
	y	0.2500	0.2500	0.2500	0.2500
	z	0.9839(3)	0.9839(3)	0.9831(3)	0.9820(3)
O1 ($4c$)	x	0.455(2)	0.459(2)	0.457(2)	0.459(2)
	y	0.2500	0.2500	0.2500	0.2500
	z	0.114(2)	0.115(2)	0.111(2)	0.117(2)
O2 ($8d$)	x	0.806(2)	0.803(2)	0.803(2)	0.807(2)
	y	0.058(1)	0.060(1)	0.058(1)	0.058(1)
	z	0.807(1)	0.804(2)	0.806(1)	0.806(1)
$\chi^2 = 1.15$		$\chi^2 = 1.27$	$\chi^2 = 1.13$	$\chi^2 = 1.05$	

crystal structure of TmFeO_3 at different temperatures are shown in Table I and they agree well with those ones in works [26] [27]. The unit cell parameter c increases monotonically with increasing temperature. The unit cell size along a and b decreases with increasing temperature up to the spin reorientation transition T_{SR} and increases monotonically above T_{SR} , which was also observed in [28, 29].

Fe^{3+} ions occupy the $4b$ position in the $Pnma$ unit cell (see Fig. 1a) and there are four types of possible collinear ordering of the Fe subsystem, which can be expressed by means of the following Bertaut notation [13]:

$$\mathbf{F} = \mathbf{S}_1 + \mathbf{S}_2 + \mathbf{S}_3 + \mathbf{S}_4,$$

$$\mathbf{C} = \mathbf{S}_1 + \mathbf{S}_2 - \mathbf{S}_3 - \mathbf{S}_4,$$

$$\mathbf{A} = \mathbf{S}_1 - \mathbf{S}_2 - \mathbf{S}_3 + \mathbf{S}_4,$$

$$\mathbf{G} = \mathbf{S}_1 - \mathbf{S}_2 + \mathbf{S}_3 - \mathbf{S}_4,$$

where \mathbf{G} describes the main antiferromagnetic component of the magnetic structure, \mathbf{F} is the ferromagnetic vector, weak antiferromagnetic components \mathbf{C} and \mathbf{A} describe the weak canting of the magnetic moments. It is convenient situation to detect the mode of magnetic alignment of elements at $4b$ site in the crystal with space group $Pnma$. In this case different magnetic modes give contributions to Bragg reflections with different parity: mode \mathbf{A} gives a contribution to reflections with $h + l$ even, k odd; \mathbf{C} – k even, $h + l$ odd; \mathbf{F} – $h + l$ even, k even; \mathbf{G} – $h + l$ odd, k odd (see Table II). $\mathbf{S}_1, \mathbf{S}_2, \mathbf{S}_3, \mathbf{S}_4$ means projections of Fe magnetic moments on arbitrary axis. In case TmFeO_3 , Fe-magnetic sublattice is ordered below temperature $T_N = 635 \text{ K}$ in a G-type structure $\Gamma 4$ (A_x, F_y, G_z). Irreducible representation $\Gamma 4$ of the space group $Pnma$ is build based on the propagation vector $\mathbf{k} = (0, 0, 0)$ and it is equivalent to $Pn'ma'$ magnetic space group (see Table III) with small spin canting

caused by the Dzyaloshinskii-Moriya (DM) interaction that induces a weak ferromagnetic (FM) moment. Spin-reorientation transition begins at decreasing temperature below $T_{SR1} = 93$ K. This transition goes through the mixed phase $\Gamma 24$ and at temperature $T_{SR2} = 83$ K the main G-type component of Fe-spins lies along the b-axis and the magnetic phase $\Gamma 2$ (C_x, G_y, F_z) is forming in the compound. Symmetry analysis [30] shows that continuous spin reorientation requires symmetry lowering at least to a monoclinic one. This statement is true only for continuous spin reorientation (i.e. for one magnetic domain where magnetic moment continuously changes direction with continuous change of temperature), while spin reorientation in TmFeO_3 has been reported in the form of changing the population of magnetic domains [31] – such mechanism of spin reorientation is compatible with orthorhombic symmetry. In our studies, we have not observed lowering orthorhombic symmetry of lattice in the spin reorientation region that is also in the agreement with [32, 33]. As discussed in [19, 34] both modes below and above the spin reorientation transition correspond to the same 'AFB' set of directions of magnetic moment. Detailed crystallographic and magnetic symmetry analysis of rare-earth orthoferrites was presented in [19] and analysis extension to (anti)ferroelectric and toroidal moments ordering was discussed in [34].

The magnetic structure was refined simultaneously for two datasets collected with different crystal orientations at $T = 20$ K without magnetic field. In magnetic neutron scattering, the magnetic form factor $F(q)$ defines the q -dependence of the magnetic scattering amplitude of a single ion in a such way that the magnetic signal at large q – large angles – is negligible in comparison with the nuclear one. Since we have no dataset above Néel temperature, in the first stage of fitting, reflections measured at theta angles greater than 60 degrees were selected from the collected dataset and the scale factor and extinction parameters were fitted. In the second stage of fitting, the remaining reflections, collected at low angles, were used to estimate the values of Fe and Tm magnetic moments. Then magnetic moments values were obtained to be equal $M_x^{Fe} = 0$, $M_y^{Fe} = 4.93(22)$, $M_z^{Fe} = -0.51(9)$ and $M_x^{Tm} = 0$, $M_y^{Tm} = 0$, $M_z^{Tm} = 0.37(8) \mu_B$ with R-factor = 11.2. The refinement with free parameters for M_x^{Fe} gives zero for these values within esds and M_y^{Tm} zero due to the symmetry restrictions, then these parameters were fixed equal to zero. Magnetic ordering of the Tm^{3+} sublattice corresponds to the irreducible representation $\Gamma 2$. The obtained magnetic moments values are in good agreement with those ones, obtained for TmFeO_3 in work [35]. Figure 1b shows the obtained magnetic structure at $T = 20$ K without magnetic field.

At the same time, X-ray measurements show that Fe^{3+} ions are not shifted from position $4b$ above as well as below spin-reorientation transition within $Pnma$ group. The treatment with lower symmetry groups did not improve the crystal structure refinement and was skipped out therefore in the ongoing discussion. This allows us

to choose Fe^{3+} as the center of the local coordinate system for determining the electric dipole moment. For that we apply the approach that was first proposed by A. K. Zvezdin in work [36] and tested on rare-earth orthochromites. As it was shown in [36], in this structure electric dipole moments can appear due to the deviation of O^{2-} ions from their high symmetry positions in the parent perovskite structure. The basic ferroelectric modes can be described in a way analogous to the magnetic modes [36]:

$$\begin{aligned}\mathbf{P} &= \mathbf{d}_1 + \mathbf{d}_2 + \mathbf{d}_3 + \mathbf{d}_4, \\ \mathbf{D} &= \mathbf{d}_1 + \mathbf{d}_2 - \mathbf{d}_3 - \mathbf{d}_4, \\ \mathbf{Q}_2 &= \mathbf{d}_1 - \mathbf{d}_2 - \mathbf{d}_3 + \mathbf{d}_4, \\ \mathbf{Q}_3 &= \mathbf{d}_1 - \mathbf{d}_2 + \mathbf{d}_3 - \mathbf{d}_4,\end{aligned}$$

where \mathbf{d}_i – electric dipole moments in the vicinity of four Fe^{3+} ions; \mathbf{P} , \mathbf{D} , \mathbf{Q}_2 , \mathbf{Q}_3 – combinations of vectors transformed by the symmetry elements of space group $Pnma$. Following this approach, the electric dipole moment for TmFeO_3 at temperatures above and below spin-reorientation transition was obtained using X-ray data. It is shown that while the magnetic moment of Fe rotates during the transition of the magnetic structure from the $\Gamma 4$ to phase $\Gamma 2$, the electric dipole moment ordering did not change. The orientation vector of the electric dipole moment has coordinates $\mathbf{r}_{EDM} = (-0.09(1), -0.98(1), -0.06(1))$ and electric dipoles ordered in antiferroelectric D mode. Figure 1c shows the arrangement of electric dipole moments in TmFeO_3 unit cell.

TABLE II: Correspondence of (anti)ferroelectric and magnetic modes in $Pnma$ crystal TmFeO_3 . Lower part of the Table show which (hkl) reflections gives intensity of each magnetic mode. "e" and "o" symbols denote even or odd parity of Miller indices, respectively.

		Fe (4b)	Tm (4c)	P	D	Q ₂	Q ₃
				F	A	C	G
\mathbf{d}_1	\mathbf{S}_1	$(0, 0, \frac{1}{2})$	$(x, \frac{1}{4}, z)$	+	+	+	+
\mathbf{d}_2	\mathbf{S}_2	$(0, \frac{1}{2}, \frac{1}{2})$	$(-x, \frac{3}{4}, -z)$	+	-	+	-
\mathbf{d}_3	\mathbf{S}_3	$(\frac{1}{2}, \frac{1}{2}, 0)$	$(-x + \frac{1}{2}, \frac{3}{4}, z + \frac{1}{2})$	+	-	-	+
\mathbf{d}_4	\mathbf{S}_4	$(\frac{1}{2}, 0, 0)$	$(x + \frac{1}{2}, \frac{1}{4}, -z + \frac{1}{2})$	+	+	-	-
				$h+l$	e	e	o
				k	e	o	o

B. Magnetic scattering dependence on magnetic field

In order to change the balance of exchange and anisotropy interactions it is possible to add an additional energy parameter to the system, such as an external magnetic field. This could lead to a change in the

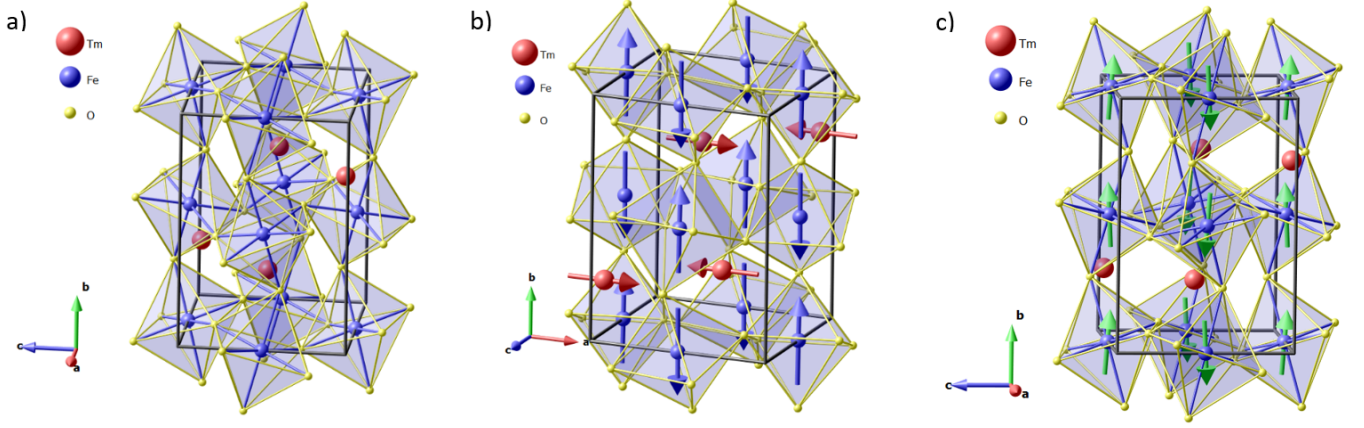


FIG. 1: TmFeO_3 structure. Red spheres are Tm ions, blue – Fe, yellow – O. Yellow lines show oxygen octahedrons around iron ions. a) Crystal structure of TmFeO_3 at $T = 300$ K; b) Magnetic structure of TmFeO_3 at $T = 20$ K. Blue arrows – direction of Fe magnetic moment, red arrows – Tm magnetic moments, the magnitude of the arrow for Tm is increased three times for convenience of demonstration; c) Antiferroelectric order of TmFeO_3 , green arrows – electric dipole moment.

TABLE III: Irreducible representations (irreps) of the space group $Pnma$ built based on the \mathbf{k} -vector equal to $(0, 0, 0)$ with corresponding magnetic space groups (MSG) and allowed magnetic modes for (4b) and (4c) Wyckoff positions.

Irrep	MSG	Fe (4b)	Tm (4c)
Γ_1	$Pnma$	(G_x, C_y, A_z)	$(0_x, C_y, 0_z)$
Γ_2	$Pn'm'a$	(C_x, G_y, F_z)	$(C_x, 0_y, F_z)$
Γ_3	$Pnm'a'$	(F_x, A_y, C_z)	$(F_x, 0_y, C_z)$
Γ_4	$Pn'ma'$	(A_x, F_y, G_z)	$(0_x, F_y, 0_z)$
Γ_5	$Pn'm'a'$	$(0_x, 0_y, 0_z)$	$(A_x, 0_y, G_z)$
Γ_6	$Pnma'$	$(0_x, 0_y, 0_z)$	$(0_x, A_y, 0_z)$
Γ_7	$Pn'ma$	$(0_x, 0_y, 0_z)$	$(0_x, G_y, 0_z)$
Γ_8	$Pnm'a$	$(0_x, 0_y, 0_z)$	$(G_x, 0_y, A_z)$

spin-reorientation transition temperature as well as to a change in the magnetic structure. Since it is convenient to follow the changes in the magnetic alignment of Fe^{3+} ions by measuring Bragg reflections with definite parity, a few reflections were chosen and were measured in the temperature range of 2 – 100 K without and with the external magnetic field applied along the b - and c -axes.

Figure 2 shows temperature dependencies two of them: reflections (-110) (G-type) and (-220) (F-type). The intensity fall at the zero field dependence of the G-type reflection in the temperature range of 83 – 93 K (Figure 2a) corresponds to the spin-reorientation transition from Γ_4 to Γ_2 phase through mixed phase Γ_{24} with the rotation of the Fe main antiferromagnetic G-type order from the c -axis to the b -axis. The effective magnetic moment in that case decreases about twice, that leads to such intensity changes. The small increase in intensity below $T \approx 40$ K is probably associated with the additional insert of the induced magnetic moment on Tm^{3+}

ions. The F-type reflection (-220) keeps its intensity at zero field temperature dependence as expected.

The application of a magnetic field in two different directions has a different effect on the temperature dependence of Bragg reflections. At the field along b -axis, intensity of G-type reflection (-110) goes to lower values in much smoother manner than it was without field, reaching lowest values at lower temperatures. It can also be seen that these lowest values are higher than that one which was observed without the field. And, at some temperatures – below 20 K for 1 T, below 40 K for 2 – 4 T – the intensity of (-110) increases considerably. The similar situation takes place for the F-type reflection (-220) that is increase of intensity at low temperatures when field was applied along b -axis (Figure 2b). The temperature behavior of these reflections at field 5.8 T looks very smooth and its intensity for (-110) does not reach such a high value, as it was observed for smaller fields.

Quite another situation was observed for the case when external magnetic field was directed along c -axis. For that field direction intensity of G-type reflection goes to minimum value at a little higher temperatures than without field. In addition, no rise of intensity was observed when temperature goes down at any field value (Figure 2c). Regarding the temperature evolution of the F-type reflection for a given field direction, it seems to be possible to estimate that there is almost no influence of the magnetic field (Figure 2d).

We connect this situation with participation of rare earth magnetic subsystem. The Tm^{3+} ion is a non-Kramers' one with two singlets in ground states and it has a highly anisotropic g -factor $g_x < 0.25$, $g_y = 8.1$ and $g_z < 0.25$ [37]. The orientation of the local coordinate system of Tm^{3+} ions is governed by the crystal field, and directly related to the tilts of oxygen octahedra. Thus, an external magnetic field directed along the

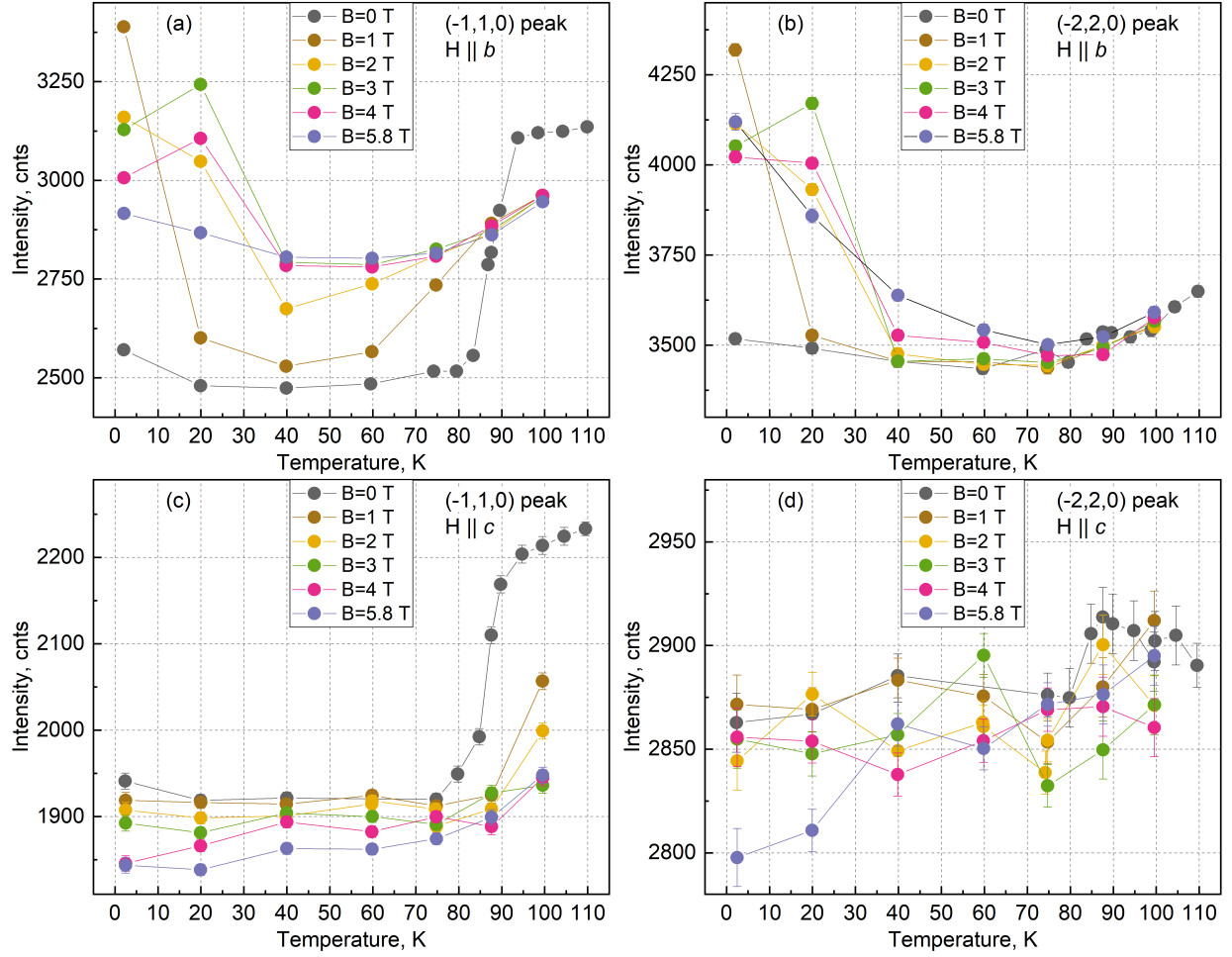


FIG. 2: Temperature dependencies of reflections intensities (-110) , (-220) for external magnetic field directed a) b) along the b -axis and c) d) along the c -axis.

b -axis induces order on magnetic moments on the Tm^{3+} ions. For the case when field is along c -axis, Tm^{3+} local susceptibility in this direction is negligible; therefore, no additional scattering is observed at Figure 2c, d. We suppose that temperature dependence of G- and F-type reflections at field 5.8 T could be related with the flop of the rare earth magnetic subsystem that is with so-called type-II switching. In type-II spin switching at a certain temperature point only moments of R^{3+} reverse thus turning parallel arrangement of Fe^{3+} and R^{3+} moments into antiparallel one or vice versa – turning antiparallel one to parallel one. Spin switching of the second type is rarely found in the RFeO_3 family. More common phenomenon is type-I spin switching where both Fe^{3+} and R^{3+} moments (induced due to superexchange interaction between Fe^{3+} and R^{3+}) are simultaneously inverted at specific temperature point. At the same time, there is report in work [38] about temperature-induced type-II spin switching in TmFeO_3 , thus one can suppose that in higher fields magnetic system of Tm^{3+} is in counterphase to Fe^{3+} one, thus producing near compensating situation.

At the low temperature and high magnetic fields we have also observed significant increase of intensity of A-type peaks (-410) , (-210) , (210) , moderate increase of intensity of (-111) and small/negligible change of intensity of (113) , (012) reflections. These changes are probably connected with the contribution from rare earth subsystem. This behavior is indirectly correlated with the data of magnetic entropy change ΔS , where the maximum of ΔS lies at 10 K in fields up to 3 T, and then shifts to the 15 – 20 K temperature range at fields over 3 T [16].

Below 40 K and above 3 T we also observed peak shifts in the omega angle from the centre of the scan window determined at 20 K without magnetic field. We interpret this as a magnetostriction effect. Interestingly, the amplitude of this shift strongly depends on the hkl indices of reflections and varies for two magnetic field directions. For the magnetic field along the c -axis we observed positive shifts for all investigated reflections with significantly higher shifts for F(1, 0, 1), A(1, 3, 1), and C(0, 2, 1) peaks. For the magnetic field along the b -axis, peaks with positive h and k show positive shift, while peaks with negative h and positive k show negative shift. Similar strong magneto-structural coupling in TmFeO_3 was reported in study [39]. It could be supposed to be a manifestation of symmetry lowering, and this should be checked in the following studies.

On the base of our observations, the magnetic phase diagram for TmFeO_3 in an external fields directed along the b -axis and the c -axis is built and presented in Figure 3. Our data did not allow us to define phase boundaries with sufficient accuracy, so the boundaries between phases are depicted rather vaguely. The points on the diagram are defined as the inflection points of the temperature dependence of the intensity. The temperature region 70 – 90 K in Figure 3a corresponds to the mixed phase Γ_{24} , which arises at the spin reorientation transition. Mag-

netic structure and spin reorientation in TmFeO_3 with-out magnetic field was examined in [14]. As it is generally accepted, spin-reorientation in RFeO_3 is closely connected with Fe-R interaction. At lower temperatures the R^{3+} ions become polarized, and at some moment the anisotropy of rare-earth subsystem overcomes the intrinsic anisotropy of the Fe system which prefers the $\Gamma_4 (A_x, F_y, G_z)$ configuration. Thus new interaction between $4f$ and $3d$ magnetic sublattices forces Fe subsystem to reorient to Γ_2 configuration. It should be noted that, within the framework of recent theoretical models, the spin reorientation transitions could be connected with more complex mechanism that results from the competition between the $4f$ - $3d$, second- and fourth-order interactions between the spin anisotropy of the $3d$ sublattice and the crystal field on rare-earth $4f$ -ions [40].

In the case when the magnetic field is directed along the c -axis, one can see that the temperature of the transition from the mixed phase Γ_{24} to phase Γ_2 increases (Figure 3b). When the field applied along c -axis, which is an antiferromagnetic axis in Γ_4 phase, it forces the Fe spins to be perpendicular to the field at some critical value H_{flop} . This latter depends on anisotropy and exchange fields, and, as one can suppose, it has the value not higher than 1 T. Thus, field applied along c -axis favors Γ_2 mode to be stabilized with lower exchange energy $J^{\text{Fe-Tm}}$, that leads to the increase of T_{SR} . So, field in c -direction increases the temperature of spin-reorientation to Γ_2 configuration, in opposite to the case of field along b -axis. As one can see from Figure 3a the temperature range of the mixed phase Γ_{24} expands to a lower temperatures. In that case, when the field directed along b -axis, that is along weak ferromagnetic component in Γ_4 , it maintains Γ_4 configuration, thus spreading region of mixed phase Γ_{24} to the lower temperatures. Similar shifts of spin reorientation temperature depending on direction of magnetic field was observed in DyFeO_3 [41, 42]. In TmFeO_3 above T_{SR} rotation of weak ferromagnetic moment in bc plane when magnetic field is applied along c -axis was confirmed using terahertz time-domain spectroscopy [43].

Regarding temperature region 2 – 30 K and field range 2 – 4 T, one can suppose, that in this case external magnetic field favors for the decoupling between Tm^{3+} and Fe^{3+} ions and Fe subsystem recover high-temperature configuration Γ_4 , while Tm subsystem remains in Γ_2 . At higher fields like 5.8 T Tm subsystem also goes to Γ_4 configuration but with ferromagnetic component directed opposite to Fe^{3+} one. Authors of [44] observed a magnetic-field-induced spin reorientation $\Gamma_2 \rightarrow \Gamma_4$ at 1.6 K in a b -cut TmFeO_3 single crystal in the static magnetic field range 2.2 – 3.6 T applied along b -axis using terahertz spectroscopy. We have also observed change of intensity of peaks at magnetic field applied along b -axis in the close field range that confirms phase transition. Situation with reverse reorientation transition without external magnetic field was observed in TbFeO_3 , a unique compound in which two types of spin reorientation from

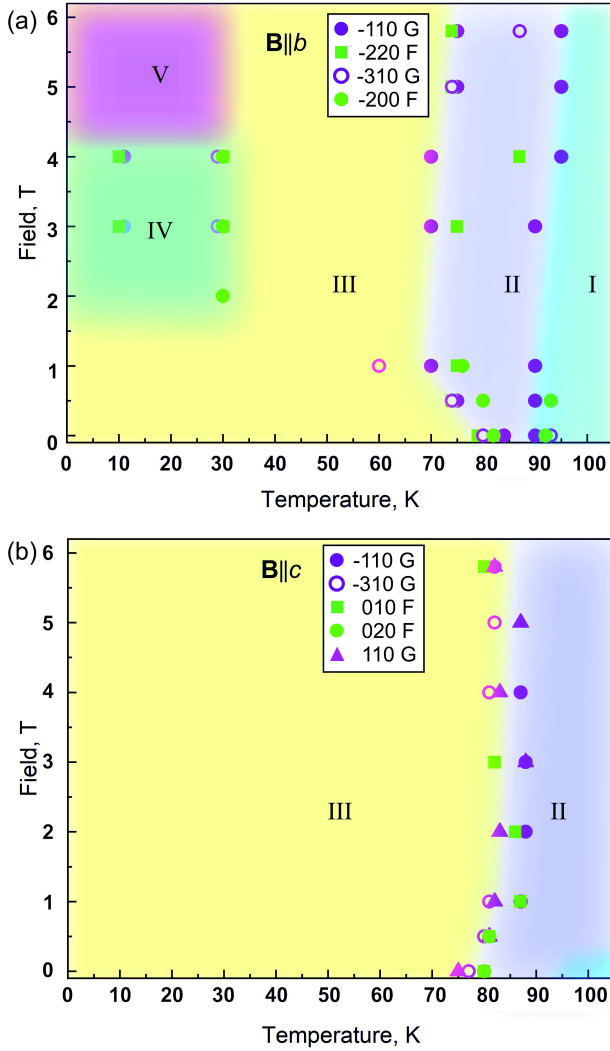


FIG. 3: Schematic of the magnetic phase diagram for TmFeO_3 a) external magnetic field along the b -axis b) along c -axis. Squares, circles and triangles are the inflection points of the temperature dependence function of the intensity for different reflections. Roman numbers designate regions corresponding by different magnetic representation: I – Γ_4 ; II – Γ_{24} ; III – Γ_2 ; IV – $\Gamma_4^{\text{Fe}} + \Gamma_2^{\text{Tm}}$; V – $\Gamma_4^{\text{Fe}} - \Gamma_2^{\text{Tm}}$.

Γ_4 to Γ_2 at 8.5 K and then Γ_2 to Γ_4 at 3 K were reported [45].

In addition, hysteresis of some peaks for the field along the b -axis was observed in the experiment, which is absent for the peaks with the field along the c -axis, i.e. along the giant magnetocaloric axis. The biggest hysteresis was observed for G-type peak $(-3, 1, 0)$, see Fig. 4, and a smaller hysteresis was observed for $G(1, 1, 0)$, $G(-1, 1, 0)$, $A(-4, 1, 0)$, $A(-2, 1, 0)$ and $F(-2, 2, 0)$ peaks (not shown). Temperature magnetization hysteresis was described using model with a few domains, which explain jump/drop of magnetization in the spin reorientation temperatures range in TmFeO_3 [31].

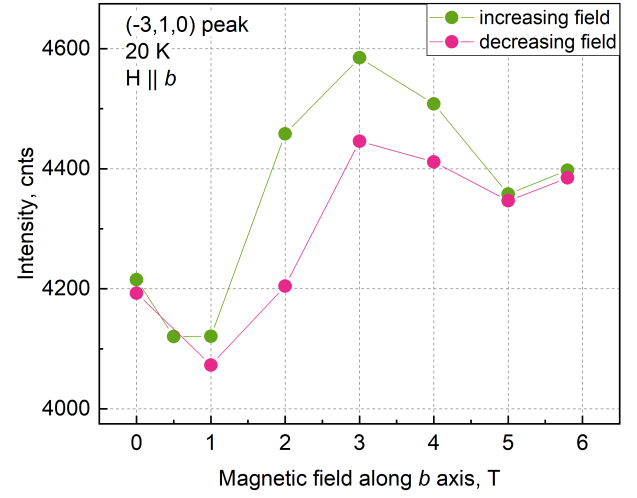


FIG. 4: Hysteresis of G-type peak $(-3, 1, 0)$ intensity in magnetic fields along the b -axis at 20 K. Error bars are of the size of the symbols.

IV. CONCLUSIONS

X-ray studies demonstrate that the lattice parameters and atomic coordinates change almost linearly in TmFeO_3 through the spin reorientation transition, keeping the orthorhombic symmetry group $Pnma$. The direction of the electric dipole moments does not change at any magnetic phase. This is additional evidence that electric system of TmFeO_3 does not have influence on the spin-reorientation transition in this compound. The main reason for the spin reorientation transition connected with superexchange interactions $4f-3d$, or with more complicate scheme of magnetic interactions [40]. Application of external magnetic field influences significantly on the spin-reorientation processes, moving the temperatures of the transitions up or low, depending on the direction of the external field. Thus, the application of the field along the c axis creates a situation favorable for the existence of the Γ_2 configuration, which leads to an increase in temperature of transition from Γ_4 to Γ_2 phase. The field along b -axis of TmFeO_3 favors for Γ_4 configuration. This result in a decrease in the transition temperature from the Γ_4 phase to the Γ_2 phase, an increase in the temperature range in which the mixed phase is observed; and also allows for the formation of new phases. At low temperatures below 20 K and fields between 2 – 4 T a new phase was observed, which has configuration supposedly Γ_4 for Fe^{3+} ions and Γ_2 for Tm^{3+} . At higher fields at these low temperatures another phase emerges with configuration Γ_4 for both Fe^{3+} subsystem and Γ_4 for Tm^{3+} , but with opposite signs.

The temperature region 2 – 30 K and field range 2 – 4 T of formation new phase are in correlation with the data on the measurement of the magnetocaloric effect, where the peak corresponding to the maximum of magnetic entropy change $\Delta S \approx 12 \text{ J/kg}\cdot\text{K}$ lies in the range

of $T = 15 - 25$ K [16].

supported by the DFG grant #SA 3688/1-1.

ACKNOWLEDGMENTS

We acknowledge Andrew Wildes (ILL) for help with crystal orientation using OrientExpress. This work was

-
- [1] R. White, Review of recent work on the magnetic and spectroscopic properties of the rare-earth orthoferrites, *Journal of Applied Physics* **40**, 1061 (1969).
 - [2] I. Dzyaloshinsky, A thermodynamic theory of “weak” ferromagnetism of antiferromagnetics, *Journal of Physics and Chemistry of Solids* **4**, 241 (1958).
 - [3] T. Moriya, Anisotropic superexchange interaction and weak ferromagnetism, *Physical Review* **120**, 91 (1960).
 - [4] S. Artyukhin, M. Mostovoy, N. P. Jensen, D. Le, K. Prokes, V. G. De Paula, H. N. Bordallo, A. Maljuk, S. Landsgesell, H. Ryll, *et al.*, Solitonic lattice and yukawa forces in the rare-earth orthoferrite TbFeO_3 , *Nature Materials* **11**, 694 (2012).
 - [5] O. Nikolov, I. Hall, S. Barilo, and S. Guretskii, A mossbauer study of temperature-driven spin-reorientation transitions in TbFeO_3 , *Journal of Physics: Condensed Matter* **6**, 3793 (1994).
 - [6] Y. Tokunaga, S. Iguchi, T.-H. Arima, and Y. Tokura, Magnetic-field-induced ferroelectric state in DyFeO_3 , *Physical Review Letters* **101**, 097205 (2008).
 - [7] Y. Tokunaga, N. Furukawa, H. Sakai, Y. Taguchi, T.-h. Arima, and Y. Tokura, Composite domain walls in a multiferroic perovskite ferrite, *Nature Materials* **8**, 558 (2009).
 - [8] Y.-Q. Song, W.-P. Zhou, Y. Fang, Y.-T. Yang, L.-Y. Wang, D.-H. Wang, and Y.-W. Du, Multiferroic properties in terbium orthoferrite, *Chinese Physics B* **23**, 077505 (2014).
 - [9] J.-H. Lee, Y. K. Jeong, J. H. Park, M.-A. Oak, H. M. Jang, J. Y. Son, and J. F. Scott, Spin-canting-induced improper ferroelectricity and spontaneous magnetization reversal in SmFeO_3 , *Physical Review Letters* **107**, 117201 (2011).
 - [10] M. Shang, C. Zhang, T. Zhang, L. Yuan, L. Ge, H. Yuan, and S. Feng, The multiferroic perovskite YFeO_3 , *Applied Physics Letters* **102**, 10.1063/1.4791697 (2013).
 - [11] A. Kimel, A. Kirilyuk, A. Tsvetkov, R. Pisarev, and T. Rasing, Laser-induced ultrafast spin reorientation in the antiferromagnet TmFeO_3 , *Nature* **429**, 850 (2004).
 - [12] A. Bombik, B. Leśniewska, J. Mayer, and A. W. Pacyna, Crystal structure of solid solutions $\text{REFe}_{1-x}(\text{Al or Ga})_x\text{O}_3$ ($\text{RE} = \text{Tb, Er, Tm}$) and the correlation between superexchange interaction $\text{Fe}^{+3} - \text{O}^{2-} - \text{Fe}^{+3}$ linkage angles and Néel temperature, *Journal of Magnetism and Magnetic Materials* **257**, 206 (2003).
 - [13] E. F. Bertaut, *Magnetism* (Academic, New York, 1963).
 - [14] J. Leake, G. Shirane, and J. Remeika, The magnetic structure of thulium orthoferrite, TmFeO_3 , *Solid State Communications* **6**, 15 (1968).
 - [15] T. Yamaguchi and K. Tsushima, Magnetic symmetry of rare-earth orthochromites and orthoferrites, *Physical Review B* **8**, 5187 (1973).
 - [16] Y.-J. Ke, X.-Q. Zhang, Y. Ma, and Z.-H. Cheng, Anisotropic magnetic entropy change in RFeO_3 single crystals ($\text{R} = \text{Tb, Tm, or Y}$), *Scientific Reports* **6**, 19775 (2016).
 - [17] S. Skorobogatov, S. E. Nikitin, K. Shaykhtudinov, A. Balaev, K. Y. Terentjev, G. Ehlers, G. Sala, E. Pomjakushina, K. Conder, and A. Podlesnyak, Low-temperature spin dynamics in the TmFeO_3 orthoferrite with a non-kramers ion, *Physical Review B* **101**, 014432 (2020).
 - [18] A. Ovsianikov, O. Usmanov, I. Zobkalo, W. Schmidt, A. Maity, V. Hutanu, E. Ressouche, K. Shaykhtudinov, K. Y. Terentjev, S. Semenov, *et al.*, Inelastic neutron studies and diffraction in magnetic fields of TbFeO_3 and YbFeO_3 , *Journal of Magnetism and Magnetic Materials* **563**, 170025 (2022).
 - [19] P. Fabrykiewicz, R. Przeniosło, and I. Sosnowska, Magnetic modes compatible with the symmetry of crystals, *Acta Crystallographica Section A: Foundations and Advances* **77**, 327 (2021).
 - [20] S. Barilo, A. Ges, S. Guretskii, D. Zhigunov, A. Ignatenko, A. Igumentsev, I. Lomako, and A. Lugnits, Seeded growth of rare-earth orthoferrites from $\text{B}_2\text{O}_3 - \text{BaF}_2 - \text{BaO}$ solvent ii. growth of high-quality RFeO_3 single crystals, *Journal of Crystal Growth* **108**, 314 (1991).
 - [21] J. Rodriguez-Cavajal, Recent developments of the program fullprof, *Comm. Powder Diffract. Newsl.* **26**, 12 (2001).
 - [22] B. Ouladdiaf, J. Archer, G. McIntyre, A. Hewat, D. Brau, and S. York, Orientexpress: A new system for laue neutron diffraction, *Physica B: Condensed Matter* **385**, 1052 (2006).
 - [23] Institut Laue-Langevin, Thermal neutron two-axis diffractometer for single-crystals D23, <https://www.ill.eu/users/instruments/instruments-list/d23/description/instrument-layout> (2023).
 - [24] N. Qureshi, Mag2pol: A program for the analysis of spherical neutron polarimetry, flipping ratio and integrated intensity data, *Journal of applied crystallography* **52**, 175 (2019).
 - [25] International tables for crystallography: Space-group symmetry (2006).
 - [26] A. Bombik, B. Leśniewska, and A. W. Pacyna, Magnetic susceptibility of powder and single-crystal TmFeO_3 orthoferrite, *Journal of Magnetism and Magnetic Materials* **214**, 243 (2000).
 - [27] M. Marezio, J. Remeika, and P. Dernier, The crystal chemistry of the rare earth orthoferrites, *Acta Crystallographica Section B: Structural Crystallography and Crystal Chemistry* **26**, 2008 (1970).

- [28] A. Bombik, H. Böhm, J. Kusz, and A. W. Pacyna, Spontaneous magnetostriction and thermal expansibility of TmFeO_3 and LuFeO_3 rare earth orthoferrites, *Journal of Magnetism and Magnetic Materials* **234**, 443 (2001).
- [29] A. A. Khan, A. Ahlawat, P. Deshmukh, M. Singh, A. Sagdeo, V. Sathe, A. Karnal, and S. Satapathy, Magneto-structural correlation across the spin reorientation transition temperature in pure and Sm substituted TmFeO_3 : A temperature dependent raman and synchrotron X-ray diffraction study, *Journal of Alloys and Compounds* **885**, 160985 (2021).
- [30] R. Przeniosło, P. Fabrykiewicz, and I. Sosnowska, Crystal symmetry aspects of materials with magnetic spin reorientation, *Acta Crystallographica Section A: Foundations and Advances* **74**, 705 (2018).
- [31] L. Tsymbal, Y. B. Bazaliy, G. Kakazei, and S. Vasiliev, Mechanisms of magnetic and temperature hysteresis in ErFeO_3 and TmFeO_3 single crystals, *Journal of Applied Physics* **108**, 10.1063/1.3499616 (2010).
- [32] L. Tsymbal, V. Kamenev, D. Khara, Y. B. Bazaliy, and P. Wigen, Structural properties of TmFeO_3 in the spontaneous reorientation region, *Low Temperature Physics* **32**, 779 (2006).
- [33] L. T. Tsymbal, Y. B. Bazaliy, V. N. Derkachenko, V. I. Kamenev, G. N. Kakazei, F. J. Palomares, and P. E. Wigen, Magnetic and structural properties of spin-reorientation transitions in orthoferrites, *Journal of Applied Physics* **101**, 123919 (2007).
- [34] P. Fabrykiewicz, R. Przeniosło, and I. Sosnowska, Magnetic, electric and toroidal polarization modes describing the physical properties of crystals. NdFeO_3 case, *Acta Crystallographica Section A: Foundations and Advances* **79**, 80 (2023).
- [35] U. Staub, L. Rettig, E. M. Bothschafter, Y. W. Windsor, M. Ramakrishnan, S. R. Avula, J. Dreiser, C. Piamonteze, V. Scagnoli, S. Mukherjee, *et al.*, Interplay of fe and tm moments through the spin-reorientation transition in TmFeO_3 , *Physical Review B* **96**, 174408 (2017).
- [36] A. Zvezdin, Z. Gareeva, and X. Chen, Multiferroic order parameters in rhombic antiferromagnets RCrO_3 , *Journal of Physics: Condensed Matter* **33**, 385801 (2021).
- [37] A. Malozemoff and R. White, Optical spectra of even-electron rare earth ions in the orthoferrites, *Solid State Communications* **8**, 665–668 (1970).
- [38] H. Song, W. Fan, R. Jia, Z. Sun, X. Ma, W. Yang, S. Zhu, B. Kang, Z. Feng, and S. Cao, Low field spin switching of single crystal TmFeO_3 , *Ceramics International* **49**, 22038 (2023).
- [39] Y. Cao, Q. Zhuang, S. Wei, X. Yin, H. Liu, Y. Zhang, Y. Kang, X. He, M. Liu, S. Cao, *et al.*, Evidence of magneto-structural coupling during the spin reorientation process in TmFeO_3 single crystal, *Journal of Magnetism and Magnetic Materials* **523**, 167626 (2021).
- [40] A. Moskvina, E. Vasinovich, and A. Shadrin, Simple realistic model of spin reorientation in $4f$ - $3d$ compounds, *Magnetochemistry* **8**, 45 (2022).
- [41] Z. Zhao, X. Zhao, H. Zhou, F. Zhang, Q. Li, C. Fan, X. Sun, and X. Li, Ground state and magnetic phase transitions of orthoferrite DyFeO_3 , *Physical Review B* **89**, 224405 (2014).
- [42] V. Eremenko, S. Gnatchenko, N. Kharchenko, P. Lebedev, K. Piotrowski, H. Szymczak, and R. Szymczak, New magnetic phase transitions in DyFeO_3 , *Europhysics Letters* **4**, 1327 (1987).
- [43] J. Guo, L. Cheng, Z. Ren, W. Zhang, X. Lin, Z. Jin, S. Cao, Z. Sheng, and G. Ma, Magnetic field tuning of spin resonance in TmFeO_3 single crystal probed with THz transient, *Journal of Physics: Condensed Matter* **32**, 185401 (2020).
- [44] N. Wang, G. Zhu, Z. Hu, X. Ju, H. Su, F. Huang, Q. Chen, Y. Cao, and X. Wang, Magnetic properties of rare-earth orthoferrites, *Infrared Phys. Technol.* **135**, 104937 (2023).
- [45] K. Belov, A. Zvezdin, and A. Mukhin, Magnetic phase transformations in Tb orthoferrites, *Zhurnal Eksperimental'noi i Teoreticheskoi Fiziki* **76**, 1100 (1979).